Climate-Resilient Nodal Power System Expansion Planning for a Realistic California Test Case

Amelia Musselman, Tomas Valencia Zuluaga, Elizabeth Glista, Minda Monteagudo, J. Michael Grappone, Matthew Signorotti, Jean-Paul Watson

[a]*Lawrence Livermore National Laboratory, 7000 East Avenue, Livermore, 94550, CA, USA*

Abstract

Climate change is increasingly impacting power system operations, not only through more frequent extreme weather events but also through shifts in routine weather patterns. Factors such as increased temperatures, droughts, changing wind patterns, and solar irradiance shifts can impact both power system production and transmission and electric load. The current power system was not designed to be resilient towards future climates. In this work, we aim to co-optimize power generation, storage, and transmission expansion in order to develop a climate-resilient system that is able to reliably meet future demands.

We analyze the impact of climate change on power systems via an adaptation of a capacity expansion planning model that seeks to minimize costs while ensuring power system resilience under a changing climate. We model the problem as a stochastic mixed-integer program, which we implement in Pyomo and solve using the stochastic programming library, mpi-sppy, along with Gurobi. We extend a synthetic but realistic, high-resolution, test case for California, the California Test System (CATS), to include parameters required for our capacity expansion planning problem and climate scenarios. Leveraging climate data from the U.S. Department of Energy's Energy Exascale Earth System Model (E3SM), we map climate projections onto power system parameters, focusing on changes in temperature, wind speed, solar irradiance, and streamflow which affect both load and wind, solar, and hydro generator availability, respectively. We compare investment decisions based on present-day climate with future-climate and find that accounting for future

This work was performed under the auspices of the U.S. Department of Energy by Lawrence Livermore National Laboratory under Contract DE-AC52-07NA27344 and was supported by the LLNL-LDRD Program under Project 22-SI-008. The authors would like to thank Gurobi for providing licenses to the Gurobi Optimizer. Additionally, we would like to thank Sofia Taylor at the University of Wisconsin-Madison for providing updates and insight about the CATS data, Juliette Franzman at Lawrence Livermore National Laboratory (LLNL) for identifying generators in the EIA data that were missing from CATS and out of service generators to remove from the CATS data, Stephen Po-Chedley at LLNL for advising on the climate data development, and Philip Cameron-Smith and Ate Visser at LLNL for advising the team on water resource restrictions.

climate scenarios significantly impacts generation, storage, and transmission investment decisions.

Keywords: OR in energy, stochastic programming, large scale optimization, power grid capacity expansion, climate resilience

---

1. Introduction

Climate change is increasingly impacting the electricity generation and transmission system not only through extreme weather events but also through routine weather patterns that are more frequently in the tail end of normal. In California, the negative impact of a more extreme climate on the grid can be observed in the recent adoption of public safety power shutoffs to mitigate potential wildfires in dry, windy conditions; wildfires caused by grid ignitions in the case when mitigation options fail or are not imposed; and forced outages, both planned and unplanned, on extreme heat days. California has also experienced ongoing drought for many years, impacting the availability of hydroelectric power, one of the few dispatchable, emissions-free resources. Furthermore, both hot and cold temperatures cause batteries, a necessary resource to satisfy ambitious clean energy goals, to lose efficiency.

More extreme climate conditions can simultaneously increase load while negatively impacting the availability and efficiency of generators, storage units, and transmission lines. Both public safety power shut-offs and unplanned outages often occur on the hottest days when people most need power for cooling. The current power system is not equipped to handle the more extreme climates observed in recent years, and operational mitigations are insufficient to support system reliability. To create a power system that is reliable and resilient to future climates, climate change must be accounted for in the power system planning stage.

The power system capacity expansion planning (CEP) problem identifies the most cost-effective combination of transmission, generation, and storage investments to simultaneously meet forecasted demand and renewable targets. By modeling this problem as a two-stage mixed-integer stochastic program with climate-informed parameters, we can plan a power system that is resilient across a wide range of climate scenarios. In this work, we seek to address the problem of power system reliability and resilience under a changing climate in the system planning stage by extending an existing stochastic capacity expansion model to account for climate impacts and solving for a large, realistic test case of California with operational scenarios based on high-resolution climate data.

1.1. Literature Review

Annually since 2022, the California Independent System Operator (CAISO), in partnership with the California Public Utilities Commission and the California Energy Commission, has released a 20-year transmission expansion plan [4]. This plan identifies the need for significant power system expansion to satisfy increasing electrification, renewable energy targets, and changes in demand due to climate change in California. However, the plan only gives recommendations for the transmission system at a high level and relies on assumptions about where future generation resources will be built. In general, although the CEP problem has been well-studied in the literature [20, 24, 27], it is common to separate the transmission, generation, and storage planning problems due to the computational challenge of solving all three systems simultaneously. The problem of transmission expansion planning (TEP) is already NP-hard due to the combinatorial nature of the decision set, i.e. how to optimally connect buses in a power network, and adding long-term climate-related uncertainty further complicates the problem. Several papers have tackled TEP with climate uncertainty via stochastic or robust optimization [39, 19]. The related problem of generation expansion planning (GEP) is also well-studied in the literature [33], including variations that account for long-term uncertainty due to climate change, fuel prices, interest rates, load growth, nuclear accident risk, and policy changes [28, 31, 46, 48].

With improvements in computational techniques for solving large mixed-integer programs (MIPs), there has been growing interest in solving power system investment models that co-optimize transmission, generation, and storage [27]. These co-optimized CEP models have been shown to significantly outperform GEP and TEP models in terms of system cost savings [25]. Additional work has studied how various modeling choices and simplifications, such as including a power flow representation or transmission line losses [64, 42], modeling short- and long-term storage [64, 35], and including generator ramping constraints [70], affect CEP results. However, most of these models have only been tested on small networks on the order of 100 buses and/or ignore uncertainty. Furthermore, even in models that consider transmission and generation simultaneously, storage is often neglected due to the added complexity of inter-connecting periods.

Even without consideration of climate-dependent uncertainties, stochastic optimization has been shown to have significant economic benefits for CEP relative to deterministic optimization and heuristic scenario planning [39]. However, solving stochastic CEP models across sufficiently many scenarios to adequately characterize the uncertainty of non-dispatchable resources and load poses additional computational challenges. In [40], the authors propose a scalable method that decom-

poses the stochastic CEP model by hour and run experiments on 8,760 one-hour scenarios that are reduced to 100-500 scenarios after clustering. Other techniques have also been developed to reduce the scenario set to a tractable size for expansion planning [36, 44, 65].

The growing impact of extreme climates on the power grid amplifies the need to consider uncertainty in long-term planning. Climate-informed CEP studies using historical reanalysis data exist [6]; however, historical data is unlikely to be sufficient for CEP, due to the long-term dynamics of climate change [21]. Other studies use future climate data or scenarios to inform CEP [2, 29, 38, 45] but at too low of a spatial representation to adequately capture climate impacts on the power grid. For example, a commonly used case-study is the 240-bus system developed in [68], which has a total of 240 buses representing the Western Electricity Coordinating Council, a reduction of two orders of magnitude from the actual system size [52]. The Electric Grid Test Cases developed at Texas A&M [51] is another set of commonly used case studies. Although this repository does contain a 10,000-bus synthetic system spanning the western United States [5], these test cases are not based on actual grid data and are not accurate representations of the power grid in the regions modeled. Although there is value in having such data sets available for research purposes, they are insufficient when location data is required to perform actual power system planning studies, especially when decisions depend on local climate conditions. The California Test System (CATS) [50] is a realistic representation of the California power grid designed for research studies that require accurate location data for power system components (see Section 3.1 for more details). Complementarily, recent advances in global circulation models combined with downscaling methods [69] allow for climate model projections with sufficient spatial and temporal resolution to be used in CEP. High-resolution weather data from these climate projections can be combined with load prediction [49, 66] and generator availability models [7] to yield input data for a CEP model.

In this paper, we extend an existing CEP model to include climate-impacted power system parameters and solve for an extension of CATS in which we add the necessary data for the climate-informed CEP model, including technoeconomic data for possible investments and load and generation availability data based on high-resolution future climate projections. To the best of our knowledge, this is the first study to solve the CEP problem on a realistically-sized system with actual substation locations and stochastic parameters based on climate forecasts for these locations.

1.2. Contributions

The contributions of this work are fourfold:

1. We extend a nodal CEP model to include climate impacts.
2. We develop a high-resolution test case, augmenting CATS with CEP data and climate scenarios representing both present day and future operating conditions.
3. We solve the stochastic program across a set of representative scenarios for the test case developed, which is a much higher-resolution instance of CEP than has previously been solved.
4. We release the data for use by the broader community.

The remainder of this paper is outlined as follows: in Section 2 we present the complete model formulation, in Section 3 we introduce the high-resolution California test case and climate data, in Section 4 we present the computational setup and results, and in Section 5 we discuss our findings.

2. Capacity Expansion Model

We build on the stochastic capacity expansion planning model from [25], making the following modifications to the model to better represent climate-impacts on capacity expansion planning:

- Modeled multiple storage types with capacity limits rather than general, unlimited storage potential. We fix the power conversion to energy capacity ratio for each storage type.
- Added transmission losses.
- Constrained generation and storage construction at each bus based on resource availability and land-use restrictions. For buses where there are no restrictions, this constraint is excluded.
- Modified the renewable portfolio standard constraint to be by scenario.[1]
- Added a location-specific and scenario-dependent availability factor for generation resources.
- Added an inter-temporal constraint on hydropower availability by bus.

We also added variable O&M costs for storage discharge and clarified some notational ambiguity in the generator and storage capacity and efficiency definitions in [25]. We exclude the disjunctive

[1]The renewable portfolio standard constraint in [25] is an expectation constraint across scenarios, which cannot be directly implemented in a decomposition of the problem via the Progressive Hedging Algorithm. While it is true that expectation constraints can be handled in a scenario decomposition methodology through dualization via Lagrangian multipliers [40], this approach can pose further challenges of parameter tuning and handling spurious losses [63]. We consider that work out of the scope of this paper and instead implement a soft constraint satisfied by scenario.

constraints that disallow simultaneous charging and discharging since they were determined to have minimal impact in [25].

The complete model formulation is presented below. Note that in the model presented here, we represent all generator types as discrete, but in the implementation, we relax some generator types to be continuous and fix some others. The actual generator construction variable types that are used in our problem instance are given in Table 4 in Section 3.2.

2.1. Nomenclature

The index sets and maps used in the model are given in Table 1.

Table 1: Index sets used in the model.

Set	**Definition**
$\mathcal{B}$	buses
$\mathcal{G}$	generator types
$\mathcal{G}^R$	renewable generator types ($\mathcal{G}^R \subseteq \mathcal{G}$)
$\mathcal{L}$	all possible transmission lines, both existing and candidate
$\mathcal{L}^0$	existing transmission lines
$\mathcal{L}^+$	candidate transmission lines
$\mathcal{S}$	storage types
$\mathcal{T}$	consecutive set of time periods used for power flow decisions ($\mathcal{T} := \{1, \ldots, T\}$)
Ω	joint load and generation availability scenarios
$o(\ell)$	origin bus of line ℓ
$d(\ell)$	destination bus of line ℓ
$\delta^+(b)$	lines originating at bus b, both existing and candidate
$\delta^-(b)$	lines terminating at bus b, both existing and candidate

The parameters used in the model are given in Table 2. Values in parentheses at the end of the parameter descriptions indicate the units. Where no value is given, the parameter is unitless.

Table 2: Parameters used in the model.

Param.	**Definition**
τ	length of each time period in the representative time horizon (h)

T^{rep}	number of times the magnitude of the representative time horizon occurs in a year. For example, if T is 24, and τ is 1 hour, T^{rep} will be 365. (y^{-1})
B_ℓ	susceptance of line ℓ (p.u.)
$C_g^{\mathcal{G}\text{-cap}}$	capital cost for generator type g, amortized over the generator lifetime (\$/MWy)
$C_\ell^{\mathcal{L}\text{-cap}}$	capital cost for a transmission line ℓ, amortized over the line lifetime (\$/y)
$C_s^{\mathcal{S}\text{-cap}}$	capital cost for power storage type s, amortized over the lifetime of a storage unit (\$/MWy of power conversion (PC) capacity)
$C_s^{\mathcal{S}-}$	discharge cost for storage type s (\$/MWh)
$C_g^{\mathcal{G}\text{-fuel}}$	fuel cost for generator type g (0 if not applicable) (\$/MWh)
C_g^{FOM}	fixed operations and maintenance cost for generator or storage type g (\$/MWy)
C_g^{VOM}	variable operations and maintenance cost for generator or storage type g (\$/MWh)
C^{RPS}	cost per unit of renewable portfolio standard violation (\$/MWh)
C^{shed}	load shedding cost (\$/MWh)
$D_{b,t,\omega}$	demand at bus b in time t and scenario ω (MW)
$H_{b,\omega}^{\max}$	maximum allowed energy output from conventional hydroelectric generation at bus b in scenario ω (MWh)
$P_g^{\mathcal{G}}$	capacity per unit of generator type g (MW)
$P_\ell^{\mathcal{L}}$	real power flow capacity for line ℓ (MW)
$P_{b,g}^{\max}$	maximum possible capacity at bus b of generator or storage type g (MW)
λ_s	hours of storage capacity for storage type s (h)
$\eta_{b,g,t,\omega}^{\mathcal{G}}$	fraction of generation capacity that is available for generator type g at bus b, time t, scenario ω
$\eta_s^{\mathcal{S}+}$	efficiency when charging storage type s
$\eta_s^{\mathcal{S}-}$	efficiency when discharging storage type s
$\eta_\ell^{\mathcal{L}}$	transmission efficiency for line ℓ
ρ^{RPS}	renewable portfolio standard, i.e. fraction of power output that must be from renewables
ρ_ω	probability of scenario ω
$X_{b,g}$	existing capacity for generator or storage type g at bus b (MW)

Note that fixed (capital and O&M) costs are given by year in order to make them on the same scale as the production cost, which we scale to a year. The capital costs are annualized using the lifetime of the plant in pre-processing. We assume generator capacities and costs are all after

generation losses. Parameters related to storage capacity are for power conversion capacity.

The variables used in the model are given in Table 3, with units indicated in parentheses.

Table 3: Decision variables used in the model.

Variable	**Definition**
$p^{\mathcal{G}}_{b,g,t,\omega}$	power output of generation type g at bus b at time t of scenario ω (MW)
$p^{\mathcal{L}+}_{\ell,t,\omega}$	power flow on line ℓ at time t of scenario ω, in the same direction as the nominal orientation of line ℓ (MW)
$p^{\mathcal{L}-}_{\ell,t,\omega}$	power flow on line ℓ at time t of scenario ω, in the opposite direction as the nominal orientation of line ℓ (MW)
p^{RPS}_{ω}	renewable portfolio standard violation in scenario ω (MW)
$p^{\text{shed}}_{b,t,\omega}$	load shed at bus b at time t of scenario ω (MW)
$p^{\mathcal{S}}_{b,s,t,\omega}$	energy storage level of type s at the end of time t at bus b in scenario ω (MWh)
$p^{\mathcal{S}+}_{b,s,t,\omega}$	power input to storage type s at bus b before losses at time t of scenario ω (MW)
$p^{\mathcal{S}-}_{b,s,t,\omega}$	power output from storage type s at bus b before losses at time t of scenario ω (MW)
$\theta_{b,t,\omega}$	phase angle at bus b at time t of scenario ω (radians)
$x^{\mathcal{G}}_{b,g}$	number of new generation units of type g at bus b
$x^{\mathcal{L}}_{\ell}$	binary variable indicating if transmission line $\ell \in \mathcal{L}^+$ is constructed
$x^{\mathcal{S}}_{b,s}$	new power conversion capacity of storage type s installed at bus b (MW)

2.2. Objective

We seek to minimize the annual capacity expansion and operations cost,

$$\begin{aligned}\min \sum_{b\in\mathcal{B}} \Bigg(\sum_{g\in\mathcal{G}} P^{\mathcal{G}}_{g}(C^{\mathcal{G}\text{-cap}}_{g} + \sum_{g\in\mathcal{G}} C^{\text{FOM}}_{g}) x^{\mathcal{G}}_{b,g} + \sum_{s\in\mathcal{S}} (C^{\mathcal{S}\text{-cap}}_{s} + C^{\text{FOM}}_{s}) x^{\mathcal{S}}_{b,s} + \sum_{g\in\mathcal{G}\cup\mathcal{S}} C^{\text{FOM}}_{g} X_{b,g} \Bigg) \\ + \sum_{\ell\in\mathcal{L}^+} C^{\mathcal{L}\text{-cap}}_{\ell} x^{\mathcal{L}}_{\ell} + T^{\text{rep}}\tau \sum_{\omega\in\Omega} \rho_{\omega} \Bigg(\sum_{t\in\mathcal{T}} \sum_{b\in\mathcal{B}} \Bigg(C^{\text{shed}} p^{\text{shed}}_{b,t,\omega} + \sum_{g\in\mathcal{G}} (C^{\text{VOM}}_{g} + C^{\mathcal{G}\text{-fuel}}_{g}) p^{\mathcal{G}}_{b,g,t,\omega} \\ + \sum_{s\in\mathcal{S}} (C^{\text{VOM}}_{s} + C^{\mathcal{S}-}_{s}) p^{\mathcal{S}-}_{b,s,t,\omega} \Bigg) + C^{\text{RPS}} p^{\text{RPS}}_{\omega} \Bigg) \end{aligned} \quad (1)$$

The first sum over buses gives the generation and storage costs that depend on capacity, specifically capital and fixed operations and maintenance (O&M) costs. Note that we only have to pay O&M costs, not capital costs, for existing generators and storage units. We could remove the O&M costs for existing systems without affecting the solution since they are fixed. However, we include

them so that the objective function represents the total annualized cost. We assume O&M costs for branches are negligible, so the sum over the capital costs of branches gives the total line cost. The sum across scenarios gives the expected cost of power output, scaled to a year. This cost is broken down into load shed, generation (variable O&M and fuel), storage discharge, and renewable portfolio standard (RPS) violation costs.

2.3. Constraints

This section defines the constraints used in the model.

2.3.1. Generation Constraints

The power generated at each bus cannot exceed the installed capacity, adjusted by the fraction of capacity that is available for the given scenario and time period,

$$p^{\mathcal{G}}_{b,g,t,\omega} \leq \eta^{\mathcal{G}}_{b,g,t,\omega}(P^{\mathcal{G}}_{g} x^{\mathcal{G}}_{b,g} + X_{b,g}) \ \forall \ b \in \mathcal{B}, g \in \mathcal{G}, t \in \mathcal{T}, \omega \in \Omega \tag{2}$$

For variable resources, such as wind and solar power, $\eta^{\mathcal{G}}_{b,g,t,\omega}$ varies by time depending on resource availability. For dispatchable resources, $\eta^{\mathcal{G}}_{b,g,t,\omega}$ is 1 unless there is a generator outage in the given scenario.

Conventional hydropower is unique in that water resources are governed by downstream water demand and safety regulations in addition to power generation needs [53]. Furthermore, although it is renewable, and the availability depends on the rainfall, streamflow, etc. in a given scenario, the reservoir level also depends on how much was consumed in previous periods. Thus, we assume that $\eta^{\mathcal{G}}_{b,hydro,t,\omega} = 1$, unless there is a generator outage, but the total output for each scenario is limited by water resource needs and availability, as given in the following constraint,

$$\tau \sum_{t \in T} p^{G}_{b,hydro,t,\omega} \leq H^{\max}_{b,\omega} \ \forall \ b \in B, \omega \in \Omega, \tag{3}$$

where *hydro* represents conventional hydroelectric generators.

We limit the maximum potential generation capacity that can be installed of each type at each bus based on resource availability and land-use restrictions,

$$P^{\mathcal{G}}_{g} x^{\mathcal{G}}_{b,g} + X_{b,g} \leq P^{\max}_{b,g} \ \forall \ b \in \mathcal{B}, g \in \mathcal{G} \tag{4}$$

2.3.2. Storage Constraints

The energy storage level cannot exceed the installed capacity,

$$p^{\mathcal{S}}_{b,s,t,\omega} \leq \lambda_s(x^{\mathcal{S}}_{b,s} + X_{b,s}) \ \forall \ s \in \mathcal{S}, t \in \mathcal{T}, \omega \in \Omega \tag{5}$$

The change in storage in a time period is limited by power conversion capacity,

$$p^{\mathcal{S}+}_{b,s,t,\omega} \leq x^{\mathcal{S}}_{b,s} + X_{b,s} \ \forall\ b \in \mathcal{B}, s \in \mathcal{S}, t \in \mathcal{T}, \omega \in \Omega \tag{6}$$

$$p^{\mathcal{S}-}_{b,s,t,\omega} \leq x^{\mathcal{S}}_{b,s} + X_{b,s} \ \forall\ b \in \mathcal{B}, s \in \mathcal{S}, t \in \mathcal{T}, \omega \in \Omega \tag{7}$$

The energy storage level changes according to the power input and output,

$$p^{\mathcal{S}}_{b,s,t,\omega} = p^{\mathcal{S}}_{b,s,t-1,\omega} + \tau(\eta^{\mathcal{S}+}_{s} p^{\mathcal{S}+}_{b,s,t,\omega} - p^{\mathcal{S}-}_{b,s,t,\omega}) \ \forall\ b \in \mathcal{B}, s \in \mathcal{S}, t \in \{2, \ldots, T\}, \omega \in \Omega \tag{8}$$

For the first period of a scenario we use the energy state of the last period of the scenario as the starting state,

$$p^{\mathcal{S}}_{b,s,1,\omega} = p^{\mathcal{S}}_{b,s,T,\omega} + \tau(\eta^{\mathcal{S}+}_{s} p^{\mathcal{S}+}_{b,s,1,\omega} - p^{\mathcal{S}-}_{b,s,1,\omega}) \ \forall\ b \in \mathcal{B}, s \in \mathcal{S}, \omega \in \Omega \tag{9}$$

Similarly to generation, for each storage type at each bus, the installed storage capacity cannot exceed the maximum allowed capacity,

$$x^{\mathcal{S}}_{b,s} + X_{b,s} \leq P^{\max}_{b,s} \ \forall\ b \in \mathcal{B}, s \in \mathcal{S} \tag{10}$$

2.3.3. Power Flow Constraints

The total power flow in either direction cannot exceed line capacity,

$$p^{\mathcal{L}+}_{\ell,t,\omega} + p^{\mathcal{L}-}_{\ell,t,\omega} \leq P^{\mathcal{L}}_{\ell} \qquad \forall\ \ell \in \mathcal{L}^0, t \in \mathcal{T}, \omega \in \Omega \tag{11}$$

$$p^{\mathcal{L}+}_{\ell,t,\omega} + p^{\mathcal{L}-}_{\ell,t,\omega} \leq P^{\mathcal{L}}_{\ell} x^{\mathcal{L}}_{\ell} \ \forall\ \ell \in \mathcal{L}^+, t \in \mathcal{T}, \omega \in \Omega \tag{12}$$

Power balance must be satisfied. Specifically, the flow into each bus plus generation and storage discharge must equal the flow out of that bus plus storage charge and demand minus load shed,

$$\begin{aligned}\sum_{\ell \in \delta^-(b)} \eta^{\mathcal{L}}_{\ell} p^{\mathcal{L}+}_{\ell,t,\omega} + \sum_{\ell \in \delta^+(b)} \eta^{\mathcal{L}}_{\ell} p^{\mathcal{L}-}_{\ell,t,\omega} + \sum_{g \in \mathcal{G}} p^{\mathcal{G}}_{b,g,t,\omega} + \sum_{s \in \mathcal{S}} \eta^{\mathcal{S}-}_{s} p^{\mathcal{S}-}_{b,s,t,\omega} \\ = \sum_{\ell \in \delta^+(b)} p^{\mathcal{L}+}_{\ell,t,\omega} + \sum_{\ell \in \delta^-(b)} p^{\mathcal{L}-}_{\ell,t,\omega} + \sum_{s \in \mathcal{S}} p^{\mathcal{S}+}_{b,s,t,\omega} + D_{b,t,\omega} - p^{\text{shed}}_{b,t,\omega} \ \forall\ b \in \mathcal{B}, t \in \mathcal{T}, \omega \in \Omega\end{aligned} \tag{13}$$

Note that we include transmission and storage losses when considering the power input to the bus.

The DC optimal power flow phase angle constraints must be satisfied for all existing lines,

$$p^{\mathcal{L}+}_{\ell,t,\omega} - p^{\mathcal{L}-}_{\ell,t,\omega} = B_{\ell}(\theta_{o(\ell),t,\omega} - \theta_{d(\ell),t,\omega}) \ \forall\ \ell \in \mathcal{L}^0, t \in \mathcal{T}, \omega \in \Omega \tag{14}$$

For candidate lines, we only enforce the constraint if the line is actually built,

$$\begin{aligned}B_{\ell}(\theta_{o(\ell),t,\omega} - \theta_{d(\ell),t,\omega}) - 2\pi|B_{\ell}|(1 - x^{\mathcal{L}}_{\ell}) \leq p^{\mathcal{L}+}_{\ell,t,\omega} - p^{\mathcal{L}-}_{\ell,t,\omega} \leq B_{\ell}(\theta_{o(\ell),t,\omega} - \theta_{d(\ell),t,\omega}) \\ + 2\pi|B_{\ell}|(1 - x^{\mathcal{L}}_{\ell}) \forall\ \ell \in \mathcal{L}^+, t \in \mathcal{T}, \omega \in \Omega\end{aligned} \tag{15}$$

Note that π is the constant ~ 3.14 here. If the line is constructed, $x^{\mathcal{L}}_{\ell}$ is 1, so Constraint 15 reduces to $p^{\mathcal{L}}_{\ell,t,\omega} = B_{\ell}(\theta_{o(\ell),t,\omega} - \theta_{d(\ell),t,\omega})$. Otherwise, $p^{\mathcal{L}}_{\ell,t,\omega}$ will be 0 due to the line capacity constraints, and the constraint reduces to, $-2\pi|B_{\ell}| \leq B_{\ell}(\theta_{o(\ell),t,\omega} - \theta_{d(\ell),t,\omega}) \leq 2\pi|B_{\ell}|$. We restrict the phase angles to be between $-\pi$ and π,

$$-\pi \leq \theta_{b,t,\omega} \leq \pi \ \forall \ b \in \mathcal{B}, t \in \mathcal{T}, \omega \in \Omega, \tag{16}$$

so $-2\pi \leq \theta_{o(\ell),t,\omega} - \theta_{d(\ell),t,\omega} \leq 2\pi$, which makes Constraint (15) valid.

2.3.4. Load Shed

Load shed cannot exceed demand,

$$p^{\text{shed}}_{b,t,\omega} \leq D_{b,t,\omega} \ \forall \ b \in \mathcal{B}, t \in \mathcal{T}, \omega \in \Omega \tag{17}$$

2.3.5. Renewable Portfolio Standards

The renewable portfolio standards must be met or a penalty paid for violations,

$$\sum_{b\in\mathcal{B}} \sum_{g\in\mathcal{G}^R} \sum_{t\in\mathcal{T}} p^{\mathcal{G}}_{b,g,t,\omega} + p^{\text{RPS}}_{\omega} \geq \rho^{\text{RPS}} \sum_{b\in\mathcal{B}} \sum_{g\in\mathcal{G}} \sum_{t\in\mathcal{T}} p^{\mathcal{G}}_{b,g,t,\omega} \ \forall \ \omega \in \Omega \tag{18}$$

2.3.6. Variable Bounds and Type Constraints

All of the operational variables are continuous, and all except the phase angles, which are bounded in Constraints 16, are restricted to be non-negative,

$$p^{\mathcal{G}}_{b,g,t,\omega} \geq 0 \ \forall \ b \in \mathcal{B}, g \in \mathcal{G}, t \in \mathcal{T}, \omega \in \Omega \tag{19}$$

$$p^{\mathcal{L}+}_{\ell,t,\omega}, p^{\mathcal{L}-}_{\ell,t,\omega} \geq 0 \ \forall \ \ell \in \mathcal{L}, t \in \mathcal{T}, \omega \in \Omega \tag{20}$$

$$p^{\text{shed}}_{b,t,\omega} \geq 0 \ \forall \ b \in \mathcal{B}, t \in \mathcal{T}, \omega \in \Omega \tag{21}$$

$$p^{\mathcal{S}}_{b,s,t,\omega}, p^{\mathcal{S}+}_{b,s,t,\omega}, p^{\mathcal{S}-}_{b,s,t,\omega} \geq 0 \ \forall \ b \in \mathcal{B}, s \in \mathcal{S}, t \in \mathcal{T}, \omega \in \Omega \tag{22}$$

Capacity expansions decisions must be non-negative. Storage investments are assumed to be continuous. Individual transmission lines are considered, so transmission expansion decision variables are binary. In the model presented here, we restrict generator investments to be integer, but in our implementation, we relax this variable to be continuous for generator types with a sufficiently small unit capacity. Additionally, generator types that we do not allow to increase (due to policy

or other restrictions) are fixed in the implementation (see Table 4).

$$x^{\mathcal{G}}_{b,g} \in \mathbf{Z}^{+} \ \forall \ g \in \mathcal{G} \tag{23}$$

$$x^{\mathcal{S}}_{b,s} \geq 0 \ \forall \ b \in \mathcal{B}, s \in \mathcal{S} \tag{24}$$

$$x^{\mathcal{L}}_{\ell} \in \{0,1\} \ \forall \ \ell \in \mathcal{L} \tag{25}$$

3. A Realistic California Test Case

We test our model on a realistically-sized test case for California with climate-informed scenarios for wind, solar, and hydro generation availability and load.

3.1. Initial System Data

The initial system data is based on the California Test System (CATS) developed in [50][2]. CATS includes actual generators, substations, and transmission lines in California and their locations, based on the U.S. Energy Information Administration's (EIA) Form EIA-860 [61] for 2019, and simulates data for parameters that are not publicly available. The original CATS data contains 8,870 buses, 3,171 of which are substations, 10,823 transmission branches, and 2,092 generators, representing the largest connected component of the California electric transmission system. In order to capture all existing generation in California, we add the generators from Form EIA-860 for 2019 that were missing from CATS to the closest substations within CATS. Additionally, we reassign solar thermal (concentrated solar power) and solar photovoltaic generator locations to be consistent with Form EIA-860 and remove generators that are out of service and not expected to return within the next year. We also remove the 3 coal generators in the system since California is moving away from coal generation. This process gives a total of 2,541 generators in the initial system data.

CATS does not distinguish storage from generation. We relabel all CATS "generators" with FuelType "Batteries" or "Hydroelectric Pumped Storage" as storage. We consider two types of batteries: 2 hour batteries and 4 hour batteries, based on Table 1 of the EIA's report addendum [57]. For pumped hydro storage, we assume 10 hours of storage capacity based on [41]. For batteries, we determine which battery type the battery in the initial system is most similar to by taking the ratio

[2]The CATS data can be downloaded from `https://github.com/WISPO-POP/CATS-CaliforniaTestSystem`. The authors directly received an update to CATS with some small corrections to the import generators, which, as of December 12, 2024, has not yet been posted to Github.

of the "Nameplate Energy Capacity (MWh)" and "Maximum Charge Rate (MW)" in the energy storage spreadsheet from Form EIA-860 [61] for 2019. We use $p_{\max}$ from the modified CATS data for the power conversion capacity and determine the energy capacity by assuming a fixed ratio of power conversion to energy capacity (1:10 for pumped hydro, 1:2 for 2 hour batteries, and 1:4 for 4 hours batteries). Figure 1 shows a map of the initial system data after these modifications.

(a) (b) (c)

Figure 1: Existing (a) generator, (b) storage, and (c) transmission line locations. The area of the circular markers is proportional to each location's installed capacity.

3.2. Expansion Data

We only allow new generators to be built at existing substations. We combine the generator types "Other Waste Biomass" and "Municipal Solid Waste" with "Landfill Gas" and combine "Other Gases" and "Other Natural Gas" with "Natural Gas Internal Combustion Engine" since our cost data is not sufficiently refined to include all of these categories. We determine whether generators are renewable or thermal and whether to model the expansion decisions as continuous, integer, or fixed based on our best judgment and the unit capacity. The average $p_{\max}$ value across existing generators of a given type in the modified CATS initial system data is used as the unit capacity for new generators. The generator types and categorizations used in our test case are shown in Table 4.

As mentioned in Section 3.1, the storage types considered are 2 hour batteries, 4 hour batteries, and hydroelectric pumped storage. All storage expansion decisions are assumed to be continuous. We assume a round-trip efficiency of 82% for batteries and 79% for hydroelectric pumped storage, based on [59] and take the square root of this value to get the charging and discharging efficiencies.

Table 4: Generator types, along with their renewable portfolio standard categories and variable types, that are considered in the model. Table also shows the abbreviations used in the results figures.

Generator Type	**Abbreviation**	**RPS Category**	**Variable Type**
Conventional Hydroelectric	Hydro	Renewable	Fixed
Petroleum Liquids	Oil	Thermal	Fixed
Natural Gas Fired Combustion Turbine	NGT	Thermal	Integer
Natural Gas Internal Combustion Engine	NGICE	Thermal	Continuous
Natural Gas Fired Combined Cycle	NGCC	Thermal	Integer
Natural Gas Steam Turbine	NGST	Thermal	Integer
Landfill Gas	Landfill	Renewable	Continuous
Geothermal	Geoth	Renewable	Integer
Nuclear	Nu	Thermal	Integer
Onshore Wind Turbine	Wind	Renewable	Continuous
Wood/Wood Waste Biomass	Biomass	Renewable	Continuous
Solar Photovoltaic - Utility Scale	Solar PV	Renewable	Continuous
Concentrated Solar Power	CSP	Renewable	Continuous
All Other	Other	Thermal	Fixed
Petroleum Coke	Coke	Thermal	Fixed
Import	Import	Thermal	Fixed

We assume that one new transmission branch, with same origin and destination, can be built everywhere where there was a transmission branch in the existing system. The same reactance, resistance, and rating as the corresponding initial system branch are used.

3.2.1. System Costs

The capital costs for each generator type are derived from the values for CAISO in Table 3 of [57]. To get the annual capital cost, amortized over the lifetime of the plant, we divide by the capital recovery factor calculated over the lifetime of the plant, as given in [58], assuming a 3% discount rate, as given in [23]. Table 1 of [57] is used to calculate the FOM and VOM costs. FOM costs are already on an annual basis and don't need to be amortized over the lifetime of the plant. Since the generator type "All Other" is not included in [57], we use fuel cells as a proxy because the

nominal capacity for fuel cells was the closest to the average capacity of "All Other" in the CATS data. We assume 0 capital and FOM costs for imports since these costs are external to the system boundary (also note that since import generators are fixed, the capital and FOM costs won't affect the solution). We take the ceiling of the maximum of the VOM cost across all other generator types for the VOM cost for imports, so the model will prioritize in-state generation over imports.

Fuel prices for natural gas and distillate fuel oil (used as a proxy for "All Other") are derived from [60]. Landfill gas is derived from [34]. All other resources (including imports) are derived from EIA's Open Data - API Query Browser [56]. These values were all given in $/million BTU. The heat rate from Table 1 of [57] was used to convert to $/kWh.

For the capital costs for candidate transmission branches, we use data from the PG&E transmission line cost calculator [43]. For lines, we use the values for "Double Circuit, Strung on both sides, Lattice Tower" under "Reconductor/Upgrade Transmission Line" since we only allow lines to be built where there is an existing transmission corridor. Costs for each line are then calculated based on the voltage and length of the line. We apply the line-length-based adjustment factors given in [43] but not those that depend on terrain and population density. For transformers, we use the costs for 3-1 Phase and 1-3 Phase "Transformer Banks" under "New Substation Equipment" in the cost calculator. If the specified transformer step does not exist, we achieve it by combining two transformers together. Similarly to generators, we amortize transmission costs over the expected lifetime of the branch, which we take to be 50 years.

Generation costs are converted to 2022 US dollars using Bureau of Labor Statistics data [54]. The transmission costs are already in 2022 USD, so no inflation adjustments are needed. We impose an RPS of 70% with a $100/MWh non-compliance cost and a $30,000/MWh load shed cost [9].

3.2.2. Maximum potential capacity

We only allow new generation capacity to be built at existing substations. Generator types labeled as "Fixed" in Table 4 are not allowed to increase from their initial system capacities due either to resource limitations (e.g. for conventional hydroelectric), policy restrictions (e.g. for petroleum liquids and petroleum coke), or being outside of the model boundary (e.g. for all other and import). Natural gas and nuclear resources are allowed to increase, although California policy discourages the expansion of these resources, because we want to allow the model to determine if expansion of these resources is necessary to balance variability in supply from renewable resources. Their use will be limited by the RPS constraint. For both natural gas and nuclear, we leave the

maximum potential capacity unconstrained at any substation for which new generation construction is allowed for wind or solar but fix the maximum to the initial system capacity wherever there are land-use restrictions (restricting the maximum potential capacity to the initial system values) on both of these resources.

To calculate the maximum potential capacity by bus for the remaining six generator types, we begin by imposing a grid over (a shapefile of) California [11], with a cell size of 0.04° by 0.04°. Grid cells are then divided into "catchment areas" using the Voronoi algorithm [3] using the centroids of grid cells containing at least one substation as poles. In the case in which a grid cell covers multiple substations, the maximum potential generation capacity within the corresponding catchment area is apportioned equally across all substations within the cell.

The U.S. Environmental Protection Agency provides a list of landfills in the United States along with data on the amount of gas generated by each landfill [62]. Any landfill with an existing landfill gas collection system (for flaring) in place is deemed a potential site for landfill gas generation.

For geothermal power, we use a shapefile containing data on the resource potential of each geothermal field [14]. Many geothermal fields do not fall completely within a single substation's catchment region, so the fields' maximum potential capacity is pro-rated proportionally to each catchment region based on the proportion of the geothermal field that overlaps with the region. Any portion of a geothermal field that is not in a geothermal protected exclusion zone [15] is considered a potential site for new geothermal power generation.

Wood/wood waste biomass has relatively low energy density, so fuel transportation is relatively expensive for this resource. To reflect this fact, we only allow biomass generators to be sited where there is already biomass available in the form of dead trees [10]. The maximum generation for a given bus is based on the number of dead trees in that substation's catchment region.

Onshore wind, solar photovoltaic (utility-scale), and concentrated solar power have the fewest siting restrictions. By default, we allow each cell to devote up to 20% of its area to each of these three generation types. We then assign each cell a Rural-Urban Commuting Area Code (RUCA) using the 2020 census blocks [55]. Any cell that does not have a valid RUCA code is given a RUCA code based on the cell's zip code [22]. Any remaining cells without valid RUCA codes are assumed to have 0 potential capacity. In this study, only utility-scale solar and wind generation expansion is considered, so any cells that fall into a metropolitan or micropolitan areas (i.e. with a RUCA code of 1 – 6) are assumed to have 0 potential capacity. Cells that fall into a small town or rural areas (RUCA codes 7 or higher) form the basis of where new Onshore Wind, Solar Photovoltaic

(utility-scale only), and concentrated solar power can be built. Each cell is then checked against the solar [12] and wind [16] Protected Area Exclusion Zones, to identify cells in which new solar and wind generation is not allowed.

For wind, solar, and biomass resources, each cell is checked against a critical habitat map [13] as well as maps of areas of conservation interest [26]. Any cell that falls within a critical habitat is assumed to have 0 potential capacity. For the remaining cells, the maximum land use is decreased proportionally to the Area of Conservation Emphasis (ACE) score from [26], where the cells with the highest local or global ACE scores are reduced to 0% land use allowed. All other cells are eligible locations for power generation construction.

Once the maximum potential generation capacities by cell have been determined, each cell is assigned to a substation (or substations) based on the substation catchment areas. The maximum potential capacity at each substation is given by the sum of the maximum potential across cells in the substation's catchment area, for each generator type. If this value is higher than the existing capacity at the substation for a given generator type, it becomes the new maximum, otherwise the maximum potential generation capacity at the given substation is equal to the existing capacity.

Lithium-ion batteries have relatively few siting restrictions [8] due to their flexible sizing and high energy densities. Thus, we do not constrain their maximum potential capacities at any bus. California has a few hydroelectric pumped storage projects in various stages of completion. We consider three that have at least preliminary filings: (1) the Eagle Mountain Pumped Storage Project [18], (2) the Fort Ross Storage Project [30], and (3) the San Vicente Energy Storage Facility [47]. The proposed capacity for these projects is used as the maximum potential capacity and assigned to the closest substation to their respective proposed locations.

3.3. Climate Scenarios

Wind and solar availability ($\eta^{\mathcal{G}}_{b,g,t,\omega}$) are obtained by performing renewable power simulations using the National Renewable Energy Laboratory's System Advisor Model (SAM) [7]. As input to SAM, hourly weather observations for 2019 and 2045 are taken from climate simulations of the SSP5-8.5 emissions scenario from the Energy Exascale Earth System Model (E3SM) California Regionally Refined Model (CARRM) [69], which features 3.25 km horizontal resolution over California. Using the default wind and solar models, `PySAM.Windpower.default("WindPowerNone")` and `PySAM.Pvsamv1.default("FlatPlatePVNone")`, we run simulations in SAM to obtain hourly power output for a simulated power plant at each substation location, after physical losses. Gen-

eration availability is then calculated by dividing these values by the nameplate capacity.

Hydropower availability is obtained from [67], which presents a water system model that intakes precipitation from climate model projections and returns projected monthly hydropower generation availability. Hydropower locations from [67] are mapped to substations in the modified CATS system based on the Form EIA-860 Name and Plant Code. For hydropower generators in the modified CATS system that are missing from [67], we use the data from the closest hydropower generator in [67], scaled by the ratio of the nameplate capacities. Monthly data from [67] is converted to daily availability by dividing by the number of days in a given month.

Load data is obtained from a multiple linear regression model based on hourly temperature [37]. We train the model on historical hourly demand from Form EIA-930 and hourly temperatures from the ERA5 reanalysis for 2018-2022. The model predicts hourly load with 5.6% error on out of sample (2023) data. For physical consistency with renewable power simulations described above, we use hourly temperatures from both historical (2019) and mid-century (2045) CARRM to generate climate-informed hourly load projections. In order to account for future changes to load from increased electrification and other policy changes, we add demand modifiers from the California Energy Commission's 2021 Integrated Energy Policy Report Mid-Mid Case.

3.4. Bus Collapsing

Initial tests indicated that very small reactance and resistance values were creating numerical instability for the test instance. In order to improve the numerical stability, we create a variation of the network in which short transmission lines and nearby buses are collapsed. To create the collapsed network, we first collapse short branches that are connected to leaf buses, i.e. buses with degree 1, based on the collapsing distance $d_{\text{br}} \geq 0$. We then collapse the remaining short branches that may be connected to buses with degree greater than 1, based on d_{br}. For each pair of buses that we merge, we define one bus to be the primary bus and the other to be the secondary bus. The new merged bus adopts the physical properties of the primary bus, and adjacent branches are treated as connecting to the primary bus (see Figure 2 for an example). We do not collapse branches that correspond to transformers.

The original CATS network has 8,870 buses and 10,162 branches, and our collapsed network has 3,972 buses and 4,757 branches for our choice of $d_{\text{br}} = 1$ km. While the original network has line resistance and reactance values as low as `6e-8` and `1e-6` p.u. respectively, the collapsed network has line resistance and reactance values on the order of `1e-5` and `1e-4` p.u. Due to

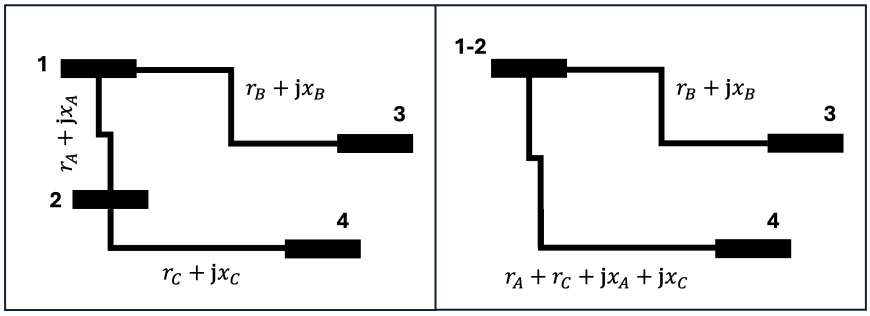

Figure 2: A simple example of a collapsed power network. The original 4-bus network is on the left. When we collapse buses 1 and 2 taking bus 1 to be the primary bus, we obtain the collapsed network on the right.

improved numerical stability in the collapsed CATS variation, we also observed faster convergence to the optimal solution for the collapsed network compared to the original network. Preliminary analysis indicates that the CEP model solved for the collapsed version of the system produces similar expansion solutions and an objective function within 0.25% of the full resolution results, with a reduction in solve time between 30-85% for the set of examined scenarios.

4. Computational Study

We implement our model in Pyomo and solve with Gurobi. We leverage the recently-developed Pyomo package mpi-sppy [32] to efficiently solve the stochastic program in a parallel computing environment. Additional details on the computational settings and adjustments made to improve model runtimes can be found in [63]. For the results presented here, Constraints (14) – (16) were relaxed, yielding a transportation approximation of the power flow model, and transmission was assumed to be lossless. We are working to develop improved solution strategies to enable the solution of the problem with a more realistic power flow representation. However, even with these simplifications, and the bus collapsing described in Section 3.4, we are still solving a much more detailed power system representation than any other capacity expansion study we are aware of.

We compare the capacity expansion solutions under present-day climate conditions, represented by climate scenarios for 2019, to the system expansion decisions under future forecasted climate conditions, represented by climate scenarios for 2045. Note that 2019 was chosen to represent present-day operations because the original CATS system is based on 2019 EIA data. Although the present-day grid should theoretically be sufficient to support present day operations, we have seen that in recent years, extreme heat events and wildfire risk have caused blackouts and public safety power shut-offs in California [1, 17]. Additionally, the RPS constraint can cause additional

capacity to be built if the variability in wind, solar, and hydro availability leads to additional capacity requirements in order to satisfy this constraint.

We start with scenarios representing hourly load, hourly wind and solar generation availability, and daily hydro for each day in 2019 and 2045 and use k-means clustering to select a subset of 20 scenarios for each year. We also compare the results from the deterministic model run for one representative day each season to the results from the stochastic program solved for the future climate case to demonstrate the importance of using stochastic programming in solving the problem.

4.1. Present Day to Future Climate Comparison

We present results for the stochastic program solved with 20 scenarios each for the 2019 and 2045 cases. Figure 3 shows the total capacity expansion for generation (a) and storage (b). Expansion is seen only in renewable resources and storage in both the 2019 and 2045 cases with more generation and storage construction required for the 2045 climate than for the 2019 climate, as expected.

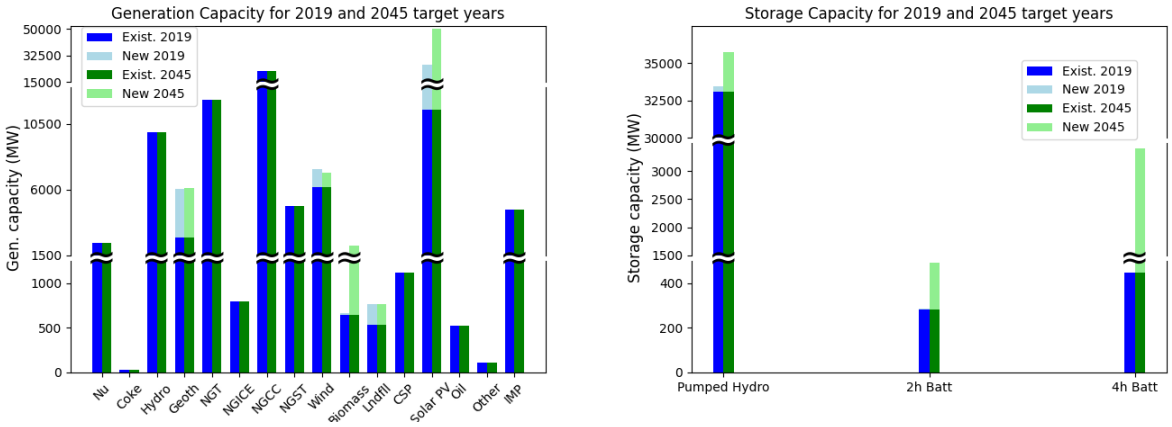

(a) (b)

Figure 3: Comparison of total generation (a) and storage (b) capacity expansion for 2019 and 2045.

Figure 4 shows the locations of new generators, storage units, and transmission lines for the 2019 case (a – c) compared to the 2045 case (d – f). We see that only sustainable generator types are built with solar and landfill gas built throughout California in both cases, although solar PV buildout is greater for 2045 than for 2019. Additionally, biomass buildout is prolific in the 2045 case. There is much more storage built for 2045 than 2019, and similarly for transmission buildout.

Figure 5 shows the expected energy output (a) and energy storage (b) across scenarios for 2019 and 2045. The expected energy output from solar PV is noticeably higher in 2045 than in 2019. Expected wind energy is also slightly higher in 2045 than 2019. The increased variability that comes

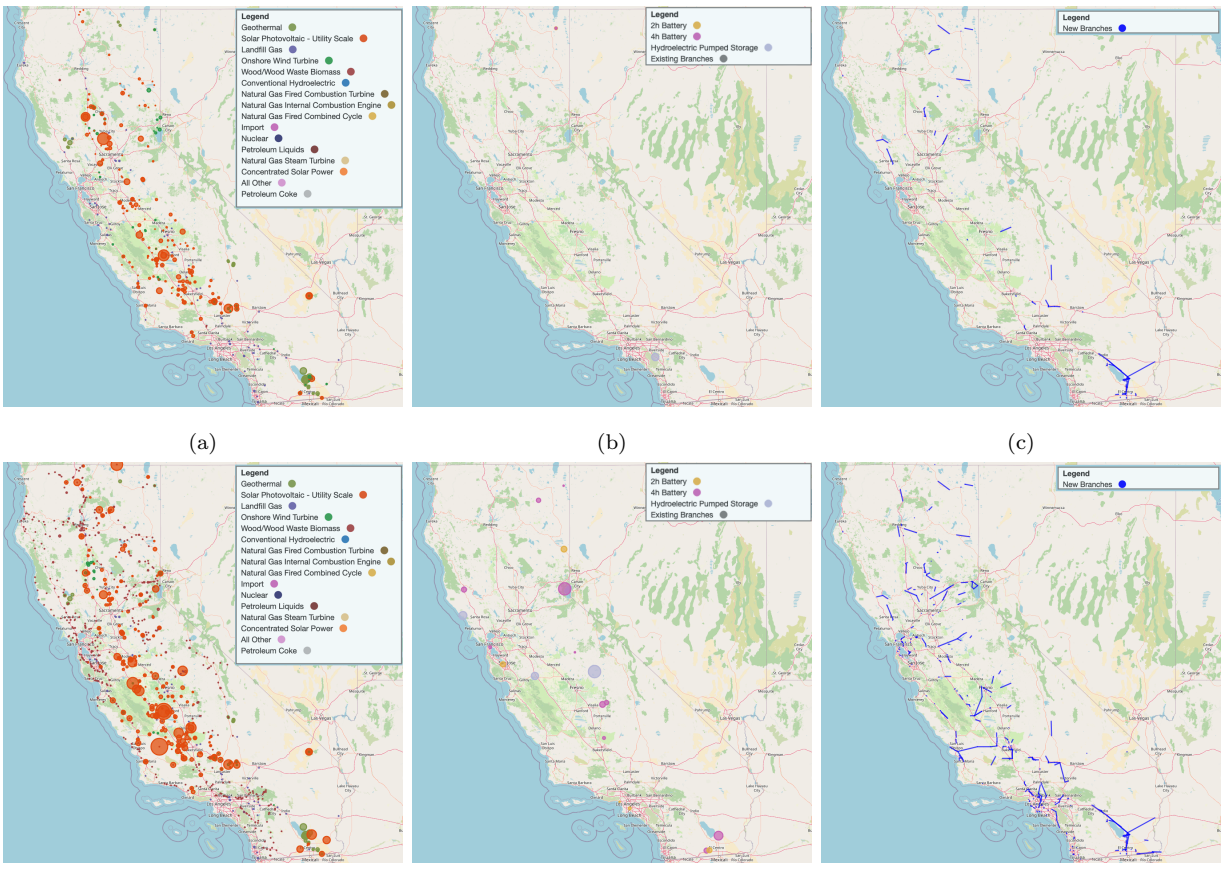

Figure 4: Comparison of new generator, storage, and transmission line locations for 2019 (a – c) and 2045 (d – f). The area of the circular markers is proportional to capacity.

with higher reliance on these generation types is balanced by increased natural gas and biomass production. Additionally, all types of storage are higher for 2045 than for 2019. CSP, hydro, and geothermal are slightly higher in 2019 than 2045, but less so than the difference in solar PV. Note that for both the 2019 and 2045 cases, an RPS target of 70% is assumed, which drives the increase in renewable capacity and energy output. However, in 2045, there is also an increase in load, which necessitates the increased production from dispatchable resources such as natural gas and biomass.

An example of operations for a day in June, 2045 is shown in Figure 6. A duck curve is observed in Figure 6a, as expected. For this representative day, solar PV is so high in the middle of the day that nuclear production is stopped. In reality, conventional nuclear reactors have long ramp times that would not allow this behavior. Ramp-up and down constraints were excluded from our model because they would increase the model complexity by connecting many time periods and adding binary variables. However, since nuclear production represents a small fraction of the total and

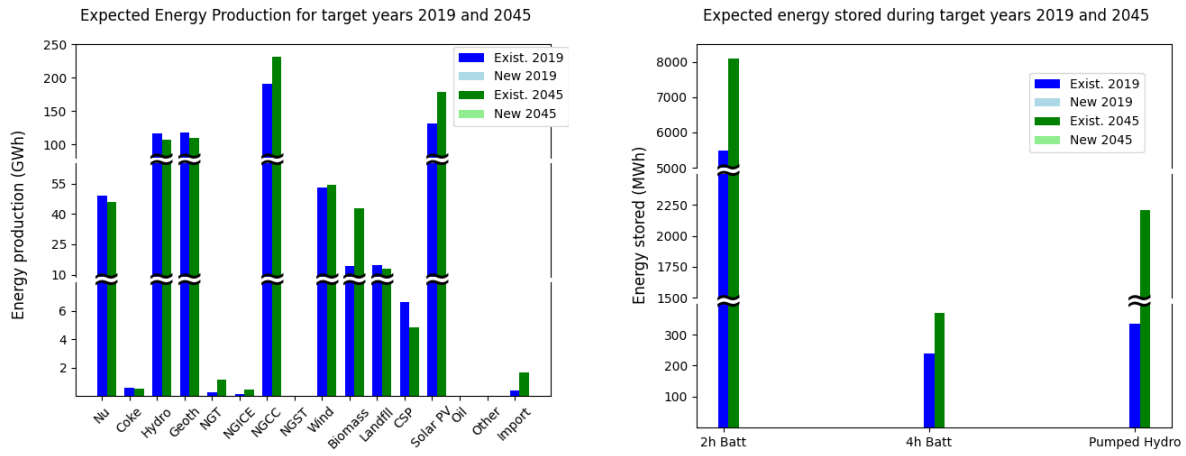

(a) (b)

Figure 5: Comparison of expected energy output (a) and energy stored (b) for 2019 and 2045.

the other resources that balance solar production can be more quickly ramped, adding ramping constraints is unlikely to affect the expansion solution significantly. More detailed power system operations studies could be performed separately given the expansion solution.

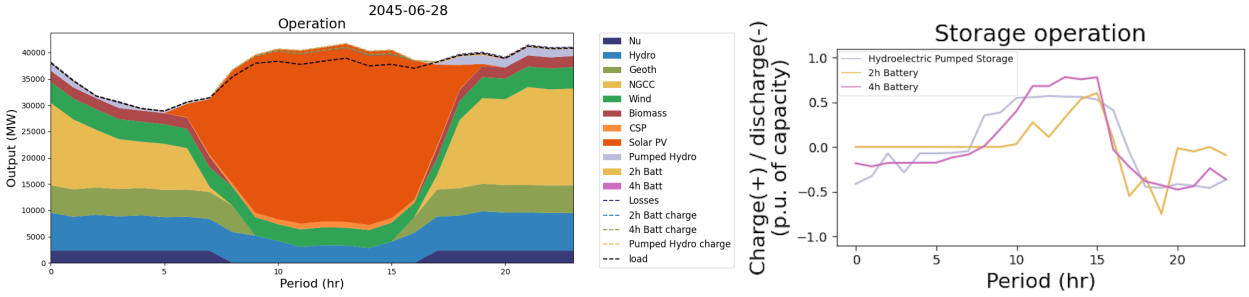

(a) (b)

Figure 6: Energy output (a) and storage operations (b) for a representative day in June, 2045. Positive values indicate charging and negative values indicate discharging in the storage plot.

Storage operations, normalized by installed storage capacity, are shown in Figure 6b. Storage operations are similar across the three types with charging during the day and discharging during the peak load hour, as expected. Looking across scenarios, we find that the power conversion capacity for batteries is governed by storage charging rather than discharging needs. In other words, the size of the inverters attached to the batteries is driven not by how much discharge is needed at the peak demand hour but by how much solar we need to take in at peak solar hour.

4.2. Deterministic to Stochastic Comparison

We compare the results from the stochastic model, solved across the 20 scenarios in 2045, to the deterministic model solved for one day in each season. Figure 7 shows the resulting total (a) generation and (b) storage capacity expansion. We see substantial differences in the expansion decisions for the stochastic case when compared to the individual scenario results, especially in solar PV and storage, emphasizing the importance of solving the problem as a stochastic program across a sufficiently representative set of scenarios.

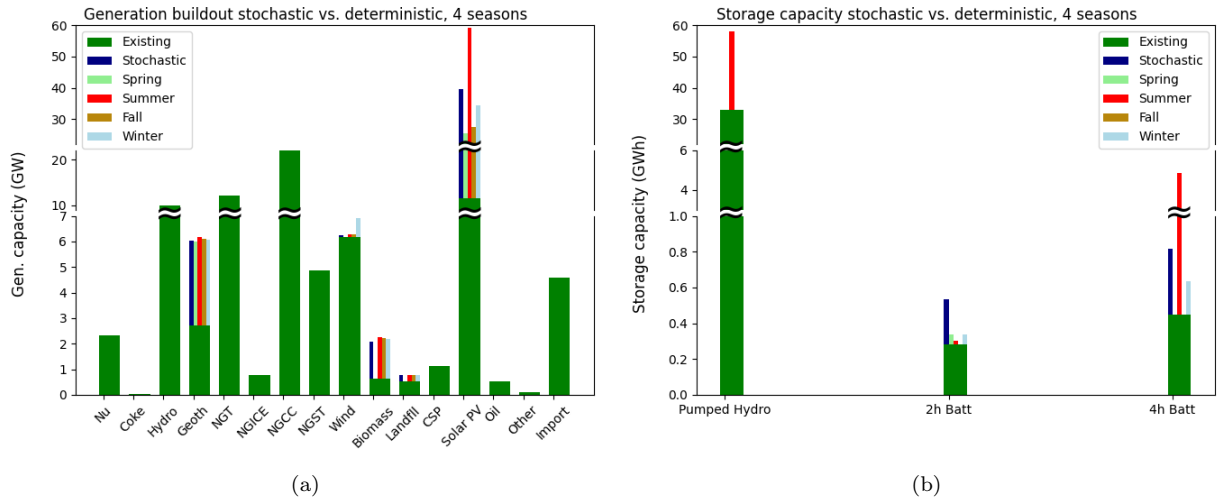

Figure 7: Comparison of total (a) generation and (b) storage capacity expansion between stochastic and deterministic model for 2045.

5. Discussion and Conclusion

We extend an existing capacity expansion planning model to include climate-impacted parameters, specifically wind, solar, and hydroelectric generation availability and load. We solve our model for a realistic representation of California of much higher resolution than has previously been solved. This research is enabled by recent advances both on the climate-data side, specifically the E3SM regionally refined model [69], and the stochastic programming side, specifically mpi-sppy [32] and our adjustments made to this library presented in earlier work [63]. To the best of our knowledge, this is the first study to co-optimize power generation, storage, and transmission at a high enough spatial and temporal resolution to make climate-informed decisions for a realistic power system.

We solve our model for a representative set of 20 generation availability and load scenarios derived from high-resolution climate forecasts representing both the present day (2019) and future

(2045). We find that the differences in climate between the present day and future cases significantly impact generation, storage, and transmission buildout. Furthermore, the expansion decisions from the stochastic program solved across 20 scenarios representing future climate conditions are significantly different from the decisions made by the deterministic model solved for individual scenarios under the same climate conditions, emphasizing the importance of using stochastic programming to solve the problem.

Realistic systems are often not well behaved, and this problem instance is no exception. In order to solve this large, realistic instance, the team had to overcome numerous numerical stability issues, which were addressed by setting values below a certain threshold to 0 and clustering buses within close proximity to each other. We are currently working to solve the problem across a larger set of scenarios spanning multiple years with more realistic power flow representations.

References

[1] ABC 7 Eyewitness News. Heat wave knocks out power to thousands of southern california homes. Accessed December 12, 2024 at `https://abc7.com/post/heat-puts-strain-socal-grid-knocks-power-thousands-homes/15278091/`.

[2] Akdemir, K. Z., Mongird, K., Kern, J. D., Oikonomou, K., Voisin, N., Burleyson, C. D., Rice, J. S., Zhao, M., Bracken, C., and Vernon, C. (2025). Investigating the effects of cooperative transmission expansion planning on grid performance during heat waves with varying spatial scales. *Applied Energy*, 378:124825.

[3] Aurenhammer, F. (1991). Voronoi diagrams–a survey of a fundamental geometric data structure. *ACM Computing Surveys*, 23(3):345–405.

[4] Billinton, J. (2024). 2024 20-Year transmission outlook. Technical report, California ISO.

[5] Birchfield, A. B., Xu, T., Gegner, K. M., Shetye, K. S., and Overbye, T. J. (2017). Grid structural characteristics as validation criteria for synthetic networks. *IEEE Transactions on Power Systems*, 32(4):3258–3265.

[6] Bissiri, M., Moura, P., Perez, R. C., Figueiredo, N. C., and da Silva, P. P. (2024). Generation capacity expansion planning with spatially-resolved electricity demand and increasing variable renewable energy supply: Perspectives from power pooling in West Africa. *Applied Energy*, 364:123115.

[7] Blair, N., DiOrio, N., Freeman, J., Gilman, P., Janzou, S., Neises, T., and Wagner, M. (2018). System Advisor Model (SAM) general description (version 2017.9.5). Technical report, National Renewable Energy Laboratory.

[8] Bowen, T., Chernyakhovskiy, I., and Denholm, P. (2019). Grid-scale battery storage frequently asked questions. Technical report, National Renewable Energy Laboratory.

[9] Brooks, D., Dudney, K., Shumavon, A., and Strauss, R. (2007). Staff recommendations on capacity market structure: A report on the August 2007 workshops in collaboration with the CAISO. Technical report, California Public Utilities Commission.

[10] Cal Fire (2023). 129 million dead trees in california. Accessed on December 22, 2023 at https://lab.data.ca.gov/dataset/129million-dead-trees-in-california.

[11] California Department of Technology (2019). CA geographic boundaries. Accessed on December 18, 2023 at https://data.ca.gov/dataset/ca-geographic-boundaries.

[12] California Energy Commission (2022). Protected areas exclusion (solar). Accessed on January 29, 2024 at https://data.ca.gov/dataset/protected-areas-exclusion-solar.

[13] California Energy Commission (2023a). Critical habitat. Accessed on January 29, 2024 at https://data.ca.gov/dataset/critical-habitat.

[14] California Energy Commission (2023b). Geothermal resource potential by field. Accessed on January 30, 2024 at https://data.ca.gov/dataset/geothermal-resource-potential-by-field.

[15] California Energy Commission (2024a). Protected areas exclusion (geothermal). Accessed January 29, 2024 at https://data.ca.gov/dataset/protected-areas-exclusion-geothermal.

[16] California Energy Commission (2024b). Protected areas exclusion (wind). Accessed January 29, 2024 at https://data.ca.gov/dataset/protected-areas-exclusion-wind.

[17] California Public Utilities Commission. Public safety power shutoffs. Accessed December 12, 2024 at https://www.cpuc.ca.gov/psps/.

[18] California State Water Resources Control Board (2020). Federal energy regulatory commission (FERC) project no. #13123. Accessed on April 30, 2024 at

https://www.waterboards.ca.gov/waterrights/water_issues/programs/water_quality_cert/eaglemtn_ferc13123.html.

[19] Chen, Y., Song, Z., and Hou, Y. (2024). Climate-adaptive transmission network expansion planning considering evolutions of resources. *IEEE Transactions on Industrial Informatics*, 20(2):2063–2078.

[20] Conejo, A. J., Baringo, L., Kazempour, S. J., and Siddiqui, A. S. (2016). *Investment in Electricity Generation and Transmission*. Springer, 1 edition.

[21] Craig, M. T. et al. (2022). Overcoming the disconnect between energy system and climate modeling. *Joule*, 6(7):1405–1417.

[22] Economic Research Service, U.S. Department of Agriculture (2019). Rural-urban commuting area codes. Accessed on September 7, 2023 at https://www.ers.usda.gov/data-products/rural-urban-commuting-area-codes/.

[23] Federal Energy Management Program (2021). 2021 discount rates. Accessed June 16, 2023 at https://www.energy.gov/sites/default/files/2021-04/2021discountrates.pdf.

[24] Gacitua, L., Gallegosa, P., Henriquez-Aubaa, R., Lorca, A., Negrete-Pincetica, M., Olivaresa, D., Valenzuela, A., and Wenzel, G. (2018). A comprehensive review on expansion planning: Models and tools for energy policy analysis. *Renewable and Sustainable Energy Reviews*, pages 346–360.

[25] Go, R. S., Muñoz, F. D., and Watson, J.-P. (2016). Assessing the economic value of co-optimized grid-scale energy storage investments in supporting high renewable portfolio standards. *Applied Energy*, pages 902–913.

[26] Gogol-Prokurat, M. (2021). Species biodiversity, areas of conservation emphasis (ACE), version 3.0. Accessed on January 17, 2024 at https://apps.wildlife.ca.gov/ace/.

[27] Gonzalez-Romero, I.-C., Wogrin, S., and Gómez, T. (2020). Review on generation and transmission expansion co-planning models under a market environment. *IET Generation, Transmission & Distribution*, pages 931–944.

[28] Gorenstin, B., Campodonico, N., Costa, J., and Pereira, M. (1993). Power system expansion planning under uncertainty. *IEEE Transactions on Power Systems*, 8(1):129–136.

[29] Handayani, K., Filatova, T., Krozer, Y., and Anugrah, P. (2020). Seeking for a climate change mitigation and adaptation nexus: Analysis of a long-term power system expansion. *Applied Energy*, 262:114485.

[30] Hydro Green Energy, LLC (2022). Before the federal energy regulatory commission united states of america application for a preliminary permit HGE energy storage 3 LLC fort ross project. Accessed on April 26, 2024 at `https://srp-prod-public-pdfs.s3-us-west-2.amazonaws.com/6GUQzYzZy-Vsb5E3djGTLp3uaxo.pdf`.

[31] Kim, D., Ryu, H., Lee, J., and Kim, K.-K. (2022). Balancing risk: Generation expansion planning under climate mitigation scenarios. *European Journal of Operational Research*, 297(2):665–679.

[32] Knueven, B., Mildebrath, D., Muir, C., Siirola, J. D., Watson, J.-P., and Woodruff, D. L. (2023). A parallel hub-and-spoke system for large-scale scenario-based optimization under uncertainty. *Math. Prog. Comp.*, 15:591—619.

[33] Koltsaklis, N. E. and Dagoumas, A. S. (2018). State-of-the-art generation expansion planning: A review. *Applied Energy*, 230:563–589.

[34] LeFevers, D. (2013). Landfill gas to renewable energy - benefits of capturing and harnessing methane emissions from municipal solid waste landfills. Technical report, Waste Management.

[35] Levin, T., Bistline, J., Sioshansi, R., Cole, W., Kwon, J., Burger, S., Crabtree, G., Jenkins, J., O'Neil, R., Korpås, M., Wogrin, S., Hobbs, B., Rosner, R., Srinivasan, V., and Botterud, A. (2023). Energy storage solutions to decarbonize electricity through enhanced capacity expansion modelling. *Nature Energy*, 8(11):1199–1208.

[36] Li, C., Conejo, A. J., Siirola, J. D., and Grossmann, I. E. (2022). On representative day selection for capacity expansion planning of power systems under extreme operating conditions. *International Journal of Electrical Power & Energy Systems*, 137:107697.

[37] Monteagudo, M. M., Po-Chedley, S., and Watson, J.-P. (2023). Population and temperature impacts on electricity demand in California. In *AGU Fall Meeting Abstracts*, volume 2023.

[38] Moreira, A., Pozo, D., Street, A., Sauma, E., and Strbac, G. (2021). Climate-aware generation and transmission expansion planning: A three-stage robust optimization approach. *European Journal of Operational Research*, 295:1099–1118.

[39] Muñoz, F. D., Hobbs, B. F., Ho, J. L., and Kasina, S. (2014). An engineering-economic approach to transmission planning under market and regulatory uncertainties: WECC case study. *IEEE Transactions on Power Systems*, 29:307–317.

[40] Muñoz, F. D. and Watson, J.-P. (2015). A scalable solution framework for stochastic transmission and generation planning problems. *Computational Management Science*, 12:491–518.

[41] National Renewable Energy Laboratory (July). 2022 v2 annual technology baseline workbook corrected 7-21-2022. Accessed on February 9, 2023 at `https://atb.nrel.gov/electricity/2022/data`.

[42] Neumann, F., Hagenmeyer, V., and Brown, T. (2022). Assessments of linear power flow and transmission loss approximations in coordinated capacity expansion problems. *Applied Energy*, 314:118859.

[43] Pacific Gas and Electric (2022). PG&E transmission line cost calculator. Accessed on June 20, 2023 at `https://www.caiso.com/InitiativeDocuments/PG&E2022DraftPerUnitCostGuide.xlsx`.

[44] Park, S., Xu, Q., and Hobbs, B. F. (2019). Comparing scenario reduction methods for stochastic transmission planning. *IET Generation, Transmission & Distribution*, 13:1005–1013.

[45] Ralston Fonseca, F., Craig, M., Jaramillo, P., Bergés, M., Severnini, E., Loew, A., Zhai, H., Cheng, Y., Nijssen, B., Voisin, N., and Yearsley, J. (2021). Effects of climate change on capacity expansion decisions of an electricity generation fleet in the southeast U.S. *Environmental Science & Technology*, 55(4):2522–2531.

[46] Raycheva, E., Schaffner, C., and Hug, G. (2022). Generation expansion planning in Switzerland considering climate change scenarios. In *2022 IEEE Power & Energy Society General Meeting*.

[47] San Diego Country Water Authority (2024). San Vicente energy storage facility. Accessed on April 20, 2024 at `https://www.sdcwa.org/projects/san-vicente-energy/`.

[48] Scott, I. J., Carvalho, P. M., Botterud, A., and Silva, C. A. (2021). Long-term uncertainties in generation expansion planning: Implications for electricity market modelling and policy. *Energy*, 227:120371.

[49] Sullivan, P., Colman, J., and Kalendra, E. (2015). Predicting the response of electricity load to climate change. Technical report, National Renewable Energy Laboratory.

[50] Taylor, S., Rangarajan, A., Rhodes, N., Snodgrass, J., Lesieutre, B. C., and Roald, L. A. (2024). California test system (CATS): A geographically accurate test system based on the california grid. *IEEE Transactions on Energy Markets, Policy and Regulation*, 2(1):107–118.

[51] Texas A&M. Electric grid test cases. Accessed on November 22, 2024 at `https://electricgrids.engr.tamu.edu/electric-grid-test-cases/`.

[52] Tomsovic, K., Zhang, X., Dimitrovski, A., and Heredia, E. Static analysis of the WECC system with continuous variable series reactor (CVSR). Accessed on November 22, 2024 at `https://arpa-e.energy.gov/sites/default/files/21_UTK_Tomosovic_GENI3.pdf`.

[53] U.S. Army Corps of Engineers (2016). Engineering and design water control management. Technical report, Department of the Army.

[54] U.S. Bureau of Labor Statistics. CPI inflation calculator. Accessed on June 16, 2023 at `https://www.bls.gov/data/inflation_calculator.htm`.

[55] U.S. Census Bureau (2022). TIGER/line shapefiles. Accessed on December 20, 2023 at `https://www.census.gov/geographies/mapping-files/2020/geo/tiger-line-file.html`.

[56] U.S. Energy Information Administration. Open data - API query browser - EIA data sets. Accessed February 8, 2023 at `https://www.eia.gov/opendata/v1/qb.php?category=40300`.

[57] U.S. Energy Information Administration (2020a). Addendum: Updated capital cost and performance characteristic estimates for utility scale electricity generating plants in the electricity market module (EMM) of the national energy modeling system (NEMS). Technical report.

[58] U.S. Energy Information Administration (2020b). Capital cost and performance characteristic estimates for utility scale electric power generating technologies. Technical report.

[59] U.S. Energy Information Administration (2021). Today in energy: Utility-scale batteries and pumped storage return about 80% of the electricity they store. Accessed on June 30, 2023 at `https://www.eia.gov/todayinenergy/detail.php?id=46756`.

[60] U.S. Energy Information Administration (2023). Short-term energy outlook. Technical report.

[61] U.S. Energy Information Administration (2024). Form EIA-860 detailed data with previous form data (EIA-860A/860B). Accessed on June 12, 2024 at `https://www.eia.gov/electricity/data/eia860/`.

[62] U.S. Environmental Protection Agency (2024). Landfill methane outreach program (LMOP). Accessed on June 4, 2024 at `https://www.epa.gov/lmop/landfill-technical-data`.

[63] Valencia Zuluaga, T., Musselman, A., Watson, J.-P., and Oren, S. S. (2024). Parallel computing for power system climate resiliency: Solving a large-scale stochastic capacity expansion problem with mpi-sppy. *Electric Power Systems Research*, 235.

[64] van Ouwerkerk, J., Gils, H. C., Gardian, H., Kittel, M., Schill, W.-P., Zerrahn, A., Murmann, A., Launer, J., Torralba-Díaz, L., and Bußar, C. (2022). Impacts of power sector model features on optimal capacity expansion: A comparative study. *Renewable and Sustainable Energy Reviews*, 157.

[65] Wang, L., McCalley, J., DeMarco, C., Akhavizadegan, F., Venkatraman, A., and Snodgrass, J. (2020). Development of expansion planning methods and tools for handling uncertainty. *Power Systems Engineering Research Center*.

[66] Wiest, P., Rudion, K., and Probst, A. (2015). Weather data-based load profile modeling for grid expansion planning. In *2015 IEEE Eindhoven PowerTech*, pages 1–6.

[67] Yates, D., Szinai, J. K., and Jones, A. D. (2024). Modeling the water systems of the western US to support climate-resilient electricity system planning. *Earth's Future*, 12.

[68] Yuan, H., Biswas, R. S., Tan, J., and Zhang, Y. (2020). Developing a reduced 240-bus WECC dynamic model for frequency response study of high renewable integration. In *2020 IEEE/PES Transmission and Distribution Conference and Exposition*, pages 1–5.

[69] Zhang, J., Bogenschutz, P., Tang, Q., Cameron-smith, P., and Zhang, C. (2024). Leveraging regional mesh refinement to simulate future climate projections for California using the simplified convection-permitting E3SM atmosphere model version 0. *Geoscientific Model Development*, 17(9):3687–3731.

[70] Zhou, Y., Zhai, Q., Yuan, W., and Wu, J. (2021). Capacity expansion planning for wind power and energy storage considering hourly robust transmission constrained unit commitment. *Applied Energy*, 302.